Research Article | Vol. 30, No. 7 / 28 Mar 2022 / Optics Express 10563
Optics EXPRESS

Spectral-temporal luminescence properties of Colloidal CdSe/ZnS Quantum Dots in relevant polymer matrices for integration in low turn-on voltage AC-driven LEDs

RICARDO M. R. ADÃO,[1] TANGYOU SUN,[1,3] BRUNO ROMEIRA,[1] PEDRO ALPUIM,[1,2] AND JANA B. NIEDER[1,*]

[1]INL - International Iberian Nanotechnology Laboratory, Headquarters at Av. Mestre Jose Veiga s/n, 4715-330 Braga, Portugal
[2]Department of Physics, University of Minho, Campus de Gualtar, 4710-057, Braga, Portugal
[3]Present address: Guangxi Key Laboratory of Precision Navigation Technology and Application, Guilin University of Electronic Technology, 541004, Guilin, China
[*]jana.nieder@inl.int

Abstract: This work employs spectral and spectral-temporal Photoluminescence (PL) spectroscopy techniques to study the radiative mechanisms in colloidal CdSe/ZnS Quantum Dot (QD) thin films without and with 1% PMMA polymer matrix embedding (QD_{PMMA}). The observed bimodal transient-spectral PL distributions reveal bandgap transitions and radiative recombinations after interdot electron transfer. The PMMA polymer embedding protects the QDs during the plasma-sputtering of inorganic layers electroluminescent (EL) devices, with minimal impact on the charge transfer properties. Further, a novel TiO_2-based, all-electron bandgap, AC-driven QLED architecture is fabricated, yielding a surprisingly low turn-on voltage, with PL-identical and narrow-band EL emission. The symmetric TiO_2 bilayer architecture is a promising test platform for alternative optical active materials.

1. Introduction

The last two decades have witnessed a ground-breaking leap in Light Emitting Devices (LEDs), especially since the 2014 Nobel prize-awarded discoveries on efficient blue-light semiconductor LEDs, which propelled the interest in both bright-lighting [1,2] and vivid-colored displays [3]. Considerable developments followed in novel nanomaterials, including Quantum Dots (QDs) [4], perovskites [5], and carbon-based materials [6]. In particular, colloidal QD exhibit stable, bright and size-dependent pure-color emission [7]. From low-cost full solution-based devices [8,9] to multicolor architectures [10], innovative designs arose for QD-based displays either as optically-pumped color-converters or full-color active electroluminescent matrices [11].

The QD-based Light Emitting Devices (QLED) properties change dramatically depending on the nature of the charge transport layers (CTL), which can be all-organic, hybrid, or all-inorganic. Over the last decade, the brightest QLED devices were achieved using hybrid organic/inorganic material-based architectures [12] that enable Direct-Current (DC) operation via dedicated electron or hole transport and injection layers. However, the longevity of organic-based devices is lowered by chemical and morphological changes in the stacked amorphous films and oxidation degradation, thus requiring inert atmospheres during fabrication and air-tight packaging to extend their operational lifetime, which increases the device costs. Contrastingly, inorganic materials are more stable and can be processed and characterized in atmospheric conditions. Inorganic (ZnO-based) electron transport layers (ETL) have been reported not only to withstand age but also to improve the device performance over time (positive aging) [13]. However, all-inorganic devices

#449037 https://doi.org/10.1364/OE.449037
Journal © 2022 Received 25 Nov 2021; revised 27 Jan 2022; accepted 4 Feb 2022; published 15 Mar 2022

Optics EXPRESS

can suffer from QD-CTL interactions, especially if both are metal oxides. The interactions can be reduced by separating the QDs from the CTL using ultrathin oxide layers [14].

CdSe/ZnS core-shell QDs are among the most popular colloidal configurations for their outstanding optical properties. While their photophysical mechanisms have been extensively studied [15], there are still unraveled interaction processes and potential opportunities to enhance and utilize their emission properties, e.g., in sensing [16] and display technologies [11]. The radiative recombination pathways in QDs combine bulk and surface state transitions [17]. In bulk (core), the highly ordered atomic arrangements lead to pure electronic (bandgap) transitions and sharp emissions. However, surface defects and dangling bonds lead to surface-state transitions and broader, redshifted emissions due to exciton trapping. In photoluminescence (PL) processes, the valence band electrons are directly photoexcited to the conduction band, leading to efficient bandgap recombinations. In electroluminescence (EL) processes, the electron-hole pair arises from external charge injection through the QD surface, making it more prone to charge trapping and surface state transitions. Such effects are tackled mainly by using a ZnS shell that passivates the surface states and protects the core from environmental changes and photo-oxidative degradation [18]. On the other hand, the deep valence band maximum of CdSe limits the hole injection, leading to accumulation at the surface [19]. The surface charging, in turn, leads to Auger recombination and field-induced charge separation [20], which reduce the luminescence yield. Strategies to balance the charge carriers include suppressing (enhancing) electron (hole) injection [21], and modulating the charge injection via organic ligands [22], and charge-generation layers [23].

Alternatively, the high electron injection efficiency in CdSe/ZnS QDs can be utilized in electron-only unipolar devices free from hole accumulation constraints. Such devices have been achieved under DC-driving [24] but are more commonly found as alternating-current (AC)-driven. The apparent disadvantage of AC-driving is the need to modulate the oscillation, which obstructs its application in battery-driven devices. On the other hand, AC devices can sustain multilayer bipolar [25–28] and far simpler unipolar insulator-QD-insulator architectures [29]. Previous works have demonstrated the use of Al_2O_3 [20,30,31], HfO_2 [30], SiO_2 [31], TaO_x [32], ZnO:SnO_2 [24] as insulator layers.

In this work, we study the optoelectric properties of colloidal CdSe/ZnS quantum dots. We use correlated spectral and time-domain spectroscopy techniques to probe QD PL processes and infer the charge recombination and transfer dynamics. Moreover, we propose, to the best of our knowledge, for the first time, a TiO_2-based electron-only insulator-QD-insulator all-inorganic, low-cost, air-stable architecture that allows validating the charge mobility observations via EL.

2. Materials and methods

2.1. PL optical characterization

2.1.1. Sample preparation

For the optical characterization, we prepared two solutions of commercial CdSe/ZnS QDs (QSP-560, Ocean Nanotech), dispersed in toluene only and toluene + 1% (v/v) Poly(methyl methacrylate) (PMMA), with a QD concentration of 10 mg/ml in both cases. The solutions were spin-coated at 1000 rpm onto glass substrates and post-baked at 100 °C for 15 minutes. For simplicity, we refer to the two QD film types as QD and QD_{PMMA}. The spinning conditions were optimized for film thicknesses of about 30 nm, measured by contact profilometry at the coating edge. After PL characterization, the samples were plasma-sputtered with 30 nm of TiO_2, and the PL spectrum was measured again.

Optics EXPRESS

2.1.2. Optical setups

Laser-scanning confocal fluorescence microscopy images (LSM-780, Zeiss) were acquired using a 458 nm excitation laser (Ar laser, max power 800 μW) and a 20x microscope objective. Fixed-power imaging and spectral measurements were collected using 1% laser power. Correlated spectral-time-domain measurements were obtained using a picosecond pulsed laser source at 467 nm (PLP-10, 80 picosecond pulse length, 20 MHz repetition rate, Hamamatsu), on a custom-built inverted confocal microscope (based on a RM21 with NanoLPS200, MadCityLabs), configured with a 480LP dichroic mirror (F38-482, AHF Analysentechnik) and an oil immersion objective (100×, NA: 1.45, 0.17 WD 0.13, Nikon CFI plan APO), signal was passed through a 473 nm long-pass filter (F76-473, AHF Analysentechnik) and coupled to a streak imaging system (Acton SP2300, Princeton Instruments spectrometer; C10910/Hamamatsu camera). .

2.2. EL optoelectric characterization

2.2.1. Sample preparation

Commercial Indium Tin Oxide (ITO)-coated glass substrates (Ossila) were partially covered with Kapton tape (for later bottom contact access) and coated with layers of 30 nm TiO_2, (plasma-sputtering), CdSe/ZnS (QD_{PMMA}) (spin-coated), 30 nm of TiO_2 (plasma-sputtering), and topped with 50 nm Au contacts (shadow-mask patterned plasma-sputtering).

2.2.2. Experimental setup

The electrical characterization was performed using a signal generator (DG1022, Rigol) and an oscilloscope (T3DS01204, Teledyne LeCroy), with a series resistor of 100 Ω. The EL measurements were collected using a fiber-coupled spectrometer (AvaSpec-ULS2048 × 64-EVO, Avantes). Electrical simulations were performed using LT-Spice with the following simulation parameters: Source: sine wave, 10 kHz frequency; Capacitor: 16.7 nF capacity; Diodes: ideal diodes of 300 (3.5 k) Ω on (off) resistance and 5.1 (∞) V forward (reverse) voltage.

3. Spectral-temporal Photoluminescence

The confocal fluorescence microscopy images in **Fig. 1**(a,b) show the spatial distribution of the PL of the spin-coated films, which we use to analyze the homogeneity, without and with polymer embedding. Contact profilometry measurements at the coating edges revealed an average 30 nm thickness for both film types. **Fig. 1(b)** displays fewer local aggregates but shows several fissures spread across the film surface. Fig. S1 of the Supplemental Document (SD) reveals a significant increase in the fissure width for a higher 10% PMMA concentration. The fissures are likely introduced by polymer shrinkage during solvent drying, commonly observed in polymeric films and structures [33]. Shrinkage effects can be reduced using specific shrinkage additives [34] or drying under controlled atmospheric conditions, such as critical-point drying [35]. Spectrally-resolved confocal fluorescence microscopy results show homogeneous wavelength distributions across the full image areas, with the film fissures showing little to no impact on the PL properties. However, the fissures may impact the EL device properties by introducing shortcircuiting sites between the flakes. Hence, the 10% PMMA concentration is discarded.

We characterize the QD photoexcitation limits by quantifying the laser power-dependent PL intensity, as shown in **Fig. 1(c)**. We observe that higher excitation laser powers lead to the exponential saturation of the PL intensity and exponential blueshift of the mean emission wavelength. The blueshift indicates an increase of bandgap transitions, which will saturate for sufficiently high power, leading to a saturation of both PL intensity and the mean wavelength. Non-radiative recombinations such as Auger relaxations eventually become dominant for high enough excitation powers, leading to the PL saturation [36]. The PL spectra in **Fig. 1(d)** show that the 1% PMMA matrix reduces the PL intensity for the QD_{PMMA} layer to 45% compared to bare

Optics EXPRESS

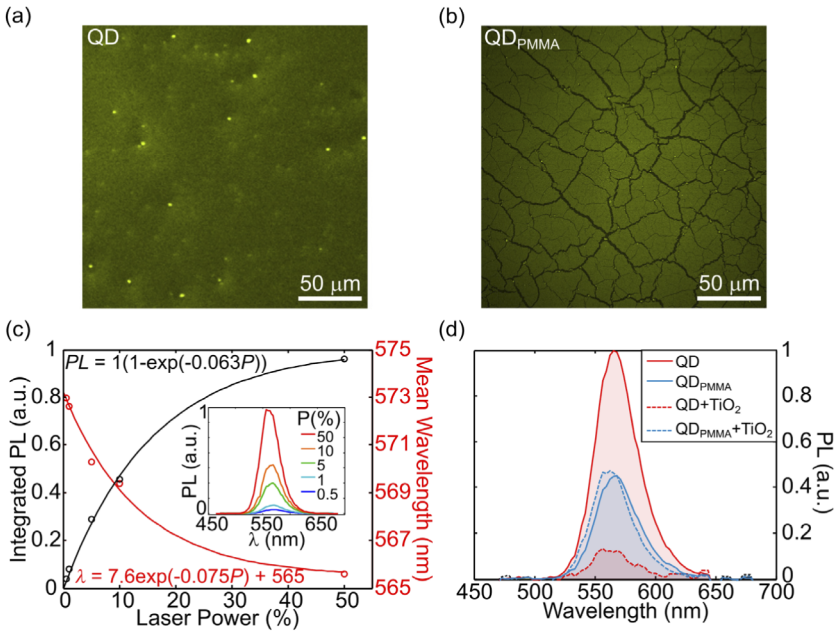

Fig. 1. Photoluminescence (PL) of CdS/ZnS QD thin films without (QD) and with (QD_{PMMA}) a 1% PMMA polymer matrix. (a-b) Confocal microscopy images. (c) PL intensity and mean wavelength (λ) dependence on excitation laser power (P). Inset: power-dependent PL spectra. (d) PL spectra comparison before and after TiO_2 plasma sputtering.

QD but has a negligible impact on the PL spectrum. Previous works have shown that amorphous polymer embeddings' chemical and dielectric properties can lead to bonds and exciton binding energy variations, leading to modified radiative and non-radiative recombination pathways [37]. In this case, the reduced PL but unchanged spectrum suggests increased non-radiative recombinations. However, when TiO_2 is sputtered on top of both films, we find an 86% PL reduction in the QD case but no PL reduction in QD_{PMMA}.

Furthermore, we observe a slight spectral blueshift and even a tiny PL increase after the TiO_2 sputtering on the QD_{PMMA} films. This observation suggests that the PMMA layer protects the QDs from plasma-induced damage, and the TiO_2 plasma-sputtering passivates surface state transitions (reduced electron charging by QD electron affinity matching the TiO_2 level) [22]. The importance of the TiO_2 sputtering process for QLED devices will impact the choice of the matrix material for the QD devices developed in this work.

The correlated spectral and time-domain PL is analyzed via confocal streak imaging, whose raw images are shown in **Fig. 2**(a-b). The measurements were performed from single points in the films after the solvent was completely dry. The spectrally-separated decay curves from **Fig. 2**(c-d) are fit with single-exponential curves for both film types, with lifetimes between 12 and 18 ns that increase with the wavelength. The overall emission profile shows a slightly longer lifetime in the QD_{PMMA}, which agrees with previous observations [38]. **Fig. 2(e)** further analyzes the same dataset by plotting the transient (time-gated) emission spectra and curve-fitting the spectral components. The dot markers represent the experimental measurements, while the lines represent the fitting results. The dashed lines represent the two Gaussian contributions per spectrum, while the full lines plot the sum of each Gaussian pair. The obtained bimodal distributions that we curve-fit using two Gaussians at (563 ± 14) and (585 ± 19) nm. Similar double Gauss curve-fittings for QD_{PMMA} can be found in Fig. S2 of the SD. We observe a decrease (increase)

Optics EXPRESS

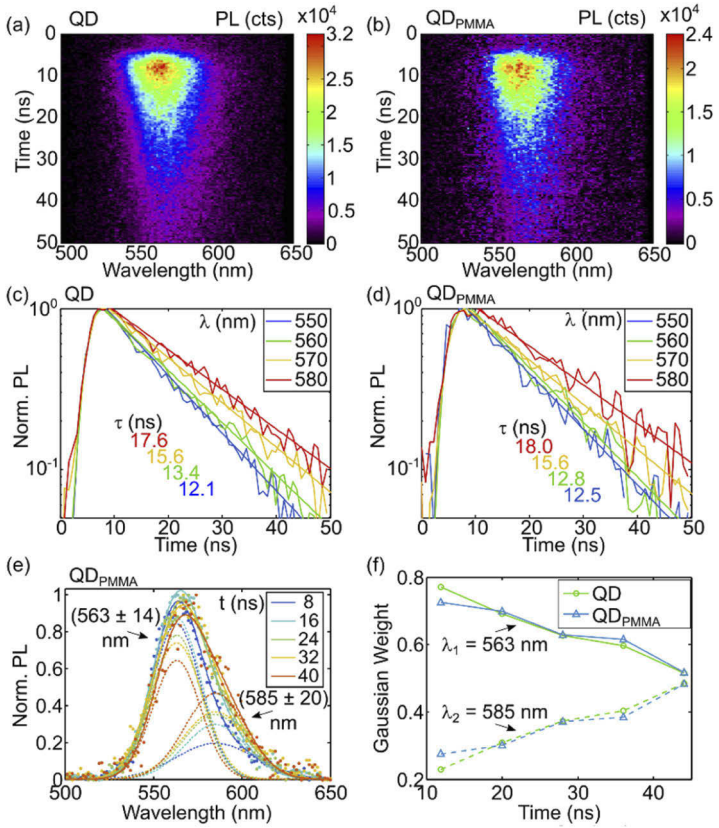

Fig. 2. Correlated temporal-spectral PL of CdS/ZnS QD thin films without (QD) and with (QD_{PMMA}) a 1% PMMA polymer matrix. (a-b) Raw streak images from QD (a) and QD_{PMMA} (b) films. (c-d) Spectrally separated PL decays and single-exponential curve-fitting (log scale). (e) Time-gated Transient PL spectra of QD_{PMMA} film. Dot markers: measured data. Dashed lines: fitted Gaussian contributions. Full lines: summed bimodal fit curve. (f) Time-dependent relative PL intensity of double-peak Gaussian curve-fitting components.

of shorter (longer) wavelength components over time for both film types, quantitatively shown in **Fig. 2(f)** where the integrated PL intensity time evolution for each contribution is plotted.

Previous works have demonstrated that interdot energy transfer in QD aggregates can lead to complex relaxation pathways and consequent multi-exponential decays. On the one hand, non-radiative recombination results in PL quenching and shorter lifetime components [39,40]. On the other hand, radiative recombination of excitons and carriers trapped at the QD boundary result in longer lifetime components [37]. While single-exponential decays are generally associated with the absence of interdot interactions, it has been previously shown [38] that simultaneous radiative and non-radiative recombinations can result in quasi-single exponential decays due to a canceling effect. From the temporal dynamics of the bimodal wavelength distribution, we believe that the longer and delayed wavelength component is associated with interdot resonant energy transfer, followed by radiative recombinations [15]. The spectrally weighted sum of all components leads to the quasi single-exponential total decay curves.

Optics EXPRESS

4. AC-driven EL assessment

We perform AC-driven EL characterization using a simple insulator-QD_{PMMA}-insulator architecture, whose bandgap diagram is shown in **Fig. 3(a)**. The QD_{PMMA} film is chosen for its higher resilience against the TiO_2 plasma sputtering and relatively unchanged optical properties relative to the QD films. TiO_2 is used for the first time as ETL in an all-electron unipolar device to the best of our knowledge. We use AC-driving with a frequency of 10 kHz, which aligns with the values used in previous works for similar architectures, ranging between 1 and 100 kHz [20,24,27,28,30–32]. **Fig. 3(b)** depicts the QLED design and the proposed equivalent electrical circuit. Whereas R_t is an actual (100 Ω) resistor in our experimental implementation, the capacitor C and "AC-diode" D_Q are virtual elements used to model the device's electrical response.

Previous works have used both series [20] and parallel [25,32,41] capacitor-based equivalent circuits to model similar systems. The experiment involves exciting the system with variable amplitude sinusoidal voltage waveforms and measuring the total current through the series resistor. The obtained I_T waveforms are shown in **Fig. 3(c).** It reveals an alternating modulation

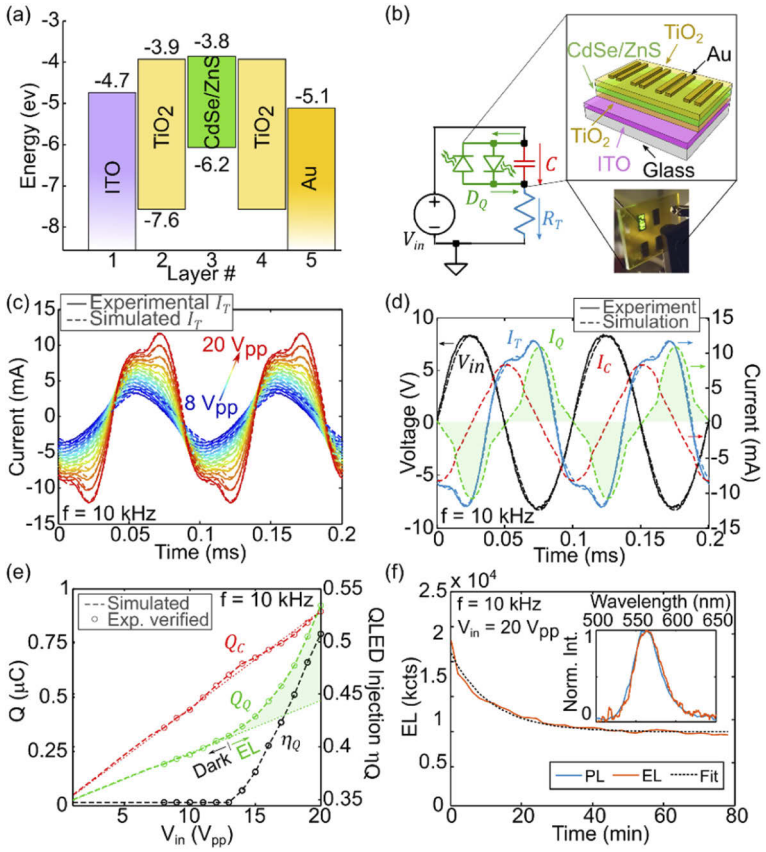

Fig. 3. Electrical characterization of AC-driven CdSe/ZnS QLED. (a) QLED material dielectric bandgap diagram. (b) QLED design, equivalent AC LED electrical circuit and photograph of the operating device. (c) Simulated and experimental input voltage (Vin)-dependent total (series) electrical current waveforms. (d) Experimental current signal decomposition into simulated equivalent circuit capacitor and QLED components. (e) Experimentally verified simulated Vin-dependent charge injection. (f) EL intensity over 80 minutes and (inset) PL versus EL spectra comparison.

Optics EXPRESS

with an additional current peak arising above a specific threshold value of the driving voltage. The SPICE simulation results, shown in **Fig. 3(d)**, demonstrate that I_T can be decomposed into two current components: I_C and I_Q, corresponding to the capacitive and QD recombination currents, respectively. The sinusoidal input voltage waveform is also shown for reference. For the simulations, we identified the diode and capacitor parameters that best fit the experimental results and obtained a capacitance of 124.8 nF/cm^2 (16.7 nF capacitor) that agrees with previously reported values [20]. We obtain an excellent overlap between simulated and experimental I_t curves for an extensive input voltage excursion range, as shown by the solid and dashed lines in **Fig. 3(c)**.

We propose using the time integrals of the absolute values of the current components, I_Q and I_C, over one period to estimate the amount of charge flowing actively, Q_Q (resulting from the recombining current in the QD), and passively, Q_C (resulting from the diffusive capacitive current) through the device:

$$Q = \int_{t_0}^{t_0+T} |I(t)|\mathrm{d}t \tag{1}$$

where Q is the total charge, t_0 is an arbitrary time-point, T is the oscillation period, $I(t)$ is the time-dependent electrical current, and t is time. This interpretation is inspired by previously reported AC-EL measurements [32], where an exponential EL burst is observed in the diode current waveform's linear region (as in **Fig. 3(d)** dashed green line). **Fig. 3(e)** shows the calculated Q_C and Q_Q, plotted as a function of the exciting voltage peak-to-peak amplitude. It can be seen that Q_C increases linearly with the input voltage excursion, and Q_Q increases linearly up to 13 V_{pp} and approximately quadratically above 13 V_{pp}. We define the charge recombination fraction as

$$Q\eta = \frac{Q_Q}{Q_Q + Q_C} \quad , \tag{2}$$

and plot it as a function of the input voltage in **Fig. 3(e)**, right y-axis. The obtained η-V plot shows values up to 50% at 20 V_{pp}, and the curve has the characteristic EL-V shape found in the literature [20], indicating the correlation between the injected charge and the electroluminescence. The 13 V_{pp} voltage threshold corresponds to the EL turn-on voltage, which was visually confirmed during the experiments, much lower than typically reported values for symmetric bandgap architectures of 110 V_{pp} (Al_2O_3) [30], 110 V_{pp} (SiO_2) [31], ~100 V_{pp} (TaO_x) [32], 80 V_{pp} (Al_2O_3) [31], 70 V_{pp} (Al_2O_3) [20], and 20 V_{pp} (ZnO:SnO_2) [24]. **Figure 3(f)** shows the EL stability over time, under a driving voltage of 20 V_{pp}. The EL drops exponentially in the first minutes of operation and then stabilizes after about 40 minutes. These observations suggest that, although an insulator, the TiO_2 acts as an efficient inorganic electron transport layer, with reduced QD-ETL QD emission-quenching interface interactions, often found in conventional inorganic ETL materials such as Zn, Cd, and Ni-based oxides [12].

We observe a perfect overlap between the EL and PL spectra (**Fig. 3(f)**, inset), suggesting similar EL and PL recombination dynamics [32]. This is interesting since the electro-excitation relies on interdot charge transfer, making it more vulnerable to surface state transitions, arguably leading to additional redshifted components in the EL spectrum, compared with the PL [17]. The EL and PL showing similar spectral components indicates similar photoelectric dynamics in both excitation processes. Hence, the 585 nm longer-lifetime PL component observed in **Fig. 2(e)** likely relates to delayed radiative recombination after interdot charge transfer (surface state transitions), which are not significantly increased by electro-excitation.

Moreover, we envision that our η-V model may be used to predict the El-V characteristics directly from the device's electrical characterization, provided that its recombination efficiency is known. The performance of our AC QLEDs is analyzed by an order-of-magnitude of the External Quantum Efficiency (EQE). The result is compared against the predictions yielded by the theoretical Internal Quantum Efficiency (IQE), obtained using the experimentally determined

Optics EXPRESS

charge injection efficiency h_Q (**Fig. 3(e)**) and PL lifetime **Fig. 2(d)**. The non-radiative Shockey-Read-Hall recombination rate and the charge carrier density at the transparency threshold are taken from the literature for similar CdSe/ZnS QD works [42]. The latter corresponds to a different QD size, but the value should still lie within the correct order of magnitude. Further, we use ray-tracing simulations to estimate our system's extraction and collection efficiencies (see Fig. S3 of the SD). Lastly, we use the Auger recombination frequency C as a fitting parameter and obtain $C = 2.0{\times}10^{-28}$ cm^{6}s^{-1} (conversely, an Auger recombination lifetime $\tau_C = 19.5$ ns). This is a relatively long Auger lifetime compared to Ref. [42], However, recent works have reported Auger lifetimes for CdSe/ZnS QDs with core and shell sizes identical to ours, where τ_C spans into the nanosecond regime [43]. Furthermore, our correlated spectral-temporal spectroscopy results (**Fig. 2** (d)) show quasi single-exponential decays with lifetimes varying only between the dominant 13 ns at the peak 560 nm emission wavelength and 18 ns at the longer 580 nm wavelength. These observations suggest a low Auger non-radiative recombination rate compared to the radiative one, and thus $\tau_C = 19.5$ ns can be considered a reasonable value. Our estimations thus yield an EQE of 0.2% at 20 V_{pp}. The obtained EQEs are relatively modest, but they agree with previous AC QLED realizations [29] that report < 1% EQE (the maximum being around 8.7%). Moreover, it is once more important to notice the very low driving voltages used in this work, roughly one order of magnitude lower than in previous works [30–32]. Using the same experimental parameters and the ray-tracing results to obtain the angle of the emission cone, we obtain a rough luminance estimate of 1500 cd/m^2.

5. Conclusion

In conclusion, we have studied the luminescence properties of commercial CdSe/ZnS QDs under photo- and electro-excitation. Spectral and time-domain observations revealed a bimodal PL spectrum composed mainly of bandgap transitions and radiative recombination after interdot electron transfer. We find that using a 1% PMMA polymer matrix protects the QDs from plasma-induced damage during the EL device insulator layer sputtering, with minimal impact on the charge transfer properties PL intensity. Such excellent optoelectronic properties hold great potential for solar cell implementations, which rely on the deposition of thick inorganic layers over the photoelectric active material. The interdot energy transfer was further analyzed via AC-driven electro-excitation using, for the first time, a TiO_2-based all-electron bandgap architecture. We find that this simple device yields a surprisingly low turn-on voltage for AC-driven EL due to the high electron injection efficiency of the CdSe/ZnS core/shell QDs, passivated with the PMMA layer. Furthermore, we obtain a PL-identical, pure-color EL emission, promising a viable all-inorganic platform for EL characterization and transparent display applications.

Funding. European Commission, Seventh Framework Programme (600375); European Commission, Horizon 2020 Framework Programme (828841); European Regional Development Fund, INTERREG V-A España-Portugal (POCTEP) 2014-2020 (0181_NANOEATERS_1_EP); CCDR-N (NORTE-01-0145-FEDER-000019); Fundação para a Ciência e a Tecnologia (UIDB/04650/2020).

Acknowledgments. We thank Riazul Arefin, who contributed to the characterization of QLED chips during his research traineeship at INL.

Disclosures. The authors declare no conflicts of interest

Data availability. Data underlying the results presented in this paper are not publicly available at this time but may be obtained from the authors upon reasonable request

Supplemental document. See Supplement 1 for supporting content.

References

1. S. Pimputkar, J. S. Speck, S. P. Denbaars, and S. Nakamura, "Prospects for LED lighting," Nat. Photonics **3**(4), 180–182 (2009).

Optics EXPRESS

2. Y. Cheng, H. Wan, T. Liang, C. Liu, M. Wu, H. Hong, K. Liu, and H. Shen, "Continuously Graded Quantum Dots: Synthesis, Applications in Quantum Dot Light-Emitting Diodes, and Perspectives," J. Phys. Chem. Lett. **12**(25), 5967–5978 (2021).
3. S. Park, Y. Xiong, R. Kim, P. Elvikis, M. Meitl, D. Kim, J. Wu, J. Yoon, C. Yu, Z. Liu, Y. Huang, K. Hwang, P. Ferreira, X. Li, K. Choquette, and J. A. Rogers, "Printed Assemblies of Inorganic Light-Emitting Diodes for Deformable and Semitransparent Displays," Science **325**(5943), 977–981 (2009).
4. B. S. Mashford, M. Stevenson, Z. Popovic, C. Hamilton, Z. Zhou, C. Breen, J. Steckel, V. Bulovic, M. Bawendi, S. Coe-Sullivan, and P. T. Kazlas, "High-efficiency quantum-dot light-emitting devices with enhanced charge injection," Nat. Photonics **7**(5), 407–412 (2013).
5. R. Wang, G. Lu, R. Zhang, and W. Xu, "Combination of the Improved Diffraction Nonlocal Boundary Condition and Three-Dimensional Wide-Angle Parabolic Equation Decomposition Model for Predicting Radio Wave Propagation," Int. J. Antennas Propag. **2017**(2728380), 1–10 (2017).
6. M. C. Chong, N. Afshar-Imani, F. Scheurer, C. Cardoso, A. Ferretti, D. Prezzi, and G. Schull, "Bright Electroluminescence from Single Graphene Nanoribbon Junctions," Nano Lett. **18**(1), 175–181 (2018).
7. Q. Sun, Y. A. Wang, L. S. Li, D. Wang, T. Zhu, J. Xu, C. Yang, and Y. Li, "Bright, multicoloured light-emitting diodes based on quantum dots," Nat. Photonics **1**(12), 717–722 (2007).
8. X. Dai, Z. Zhang, Y. Jin, Y. Niu, H. Cao, X. Liang, L. Chen, J. Wang, and X. Peng, "Solution-processed, high-performance light-emitting diodes based on quantum dots," Nature **515**(7525), 96–99 (2014).
9. Y. Fu, D. Kim, H. Moon, H. Yang, and H. Chae, "Hexamethyldisilazane-mediated, full-solution-processed inverted quantum dot-light-emitting diodes," J. Mater. Chem. C **5**(3), 522–526 (2017).
10. H. Zhang, Q. Su, and S. Chen, "Quantum-dot and organic hybrid tandem light-emitting diodes with multi-functionality of full-color-tunability and white-light-emission," Nat. Commun. **11**(1), 2826 (2020).
11. Y. M. Huang, K. J. Singh, A. C. Liu, C. C. Lin, Z. Chen, K. Wang, Y. Lin, Z. Liu, T. Wu, and H. C. Kuo, "Advances in quantum-dot-based displays," Nanomaterials **10**(7), 1327 (2020).
12. Q. Yuan, T. Wang, P. Yu, H. Zhang, H. Zhang, and W. Ji, "A review on the electroluminescence properties of quantum-dot light-emitting diodes," Org. Electron. **90**, 106086 (2021).
13. Q. Su, H. Zhang, Y. Sun, X. W. Sun, and S. Chen, "Enhancing the Performance of Quantum-Dot Light-Emitting Diodes by Postmetallization Annealing," ACS Appl. Mater. Interfaces **10**(27), 23218–23224 (2018).
14. W. Ji, S. Liu, H. Zhang, R. Wang, W. Xie, and H. Zhang, "Ultrasonic Spray Processed, Highly Efficient All-Inorganic Quantum-Dot Light-Emitting Diodes," ACS Photonics **4**(5), 1271–1278 (2017).
15. H. Xu, V. Chmyrov, J. Widengren, H. Brismar, and Y. Fu, "Mechanisms of fluorescence decays of colloidal CdSe-CdS/ZnS quantum dots unraveled by time-resolved fluorescence measurement," Phys. Chem. Chem. Phys. **17**(41), 27588–27595 (2015).
16. K. Chou and A. Dennis, "Förster Resonance Energy Transfer between Quantum Dot Donors and Quantum Dot Acceptors," Sensors **15**(6), 13288–13325 (2015).
17. W. W. Zhao, J. Wang, Y. C. Zhu, J. J. Xu, and H. Y. Chen, "Quantum Dots: Electrochemiluminescent and Photoelectrochemical Bioanalysis," Anal. Chem. **87**(19), 9520–9531 (2015).
18. X. Wang, J. Yu, and R. Chen, "Optical Characteristics of ZnS Passivated CdSe/CdS Quantum Dots for High Photostability and Lasing," Sci. Rep. **8**(1), 17323–17327 (2018).
19. S. Chen, W. Cao, T. Liu, S. W. Tsang, Y. Yang, X. Yan, and L. Qian, "On the degradation mechanisms of quantum-dot light-emitting diodes," Nat. Commun. **10**(1), 1–9 (2019).
20. D. Bozyigit, V. Wood, Y. Shirasaki, and V. Bulovic, "Study of field driven electroluminescence in colloidal quantum dot solids Study of field driven electroluminescence in colloidal quantum dot solids," J. Appl. Phys. **111**(11), 113701 (2012).
21. Q. Su, H. Zhang, and S. Chen, "Identification of excess charge carriers in InP-based quantum-dot light-emitting diodes," Appl. Phys. Lett. **117**(5), 053502 (2020).
22. S. H. Kang, C. K. Kumar, Z. Lee, V. Radmilovic, and E. T. Kim, "Effects of surface ligands on the charge memory characteristics of CdSe/ZnS nanocrystals in TiO2 thin film," Appl. Phys. Lett. **95**(18), 183111–183114 (2009).
23. N. Zhang, H. Tang, K. Shi, W. Wang, W. Deng, B. Xu, K. Wang, and X. W. Sun, "High-performance all-solution-processed quantum dot near-infrared-to-visible upconversion devices for harvesting photogenerated electrons," Appl. Phys. Lett. **115**(22), 221103 (2019).
24. V. Wood, M. J. Panzer, J. M. Caruge, J. E. Halpert, M. G. Bawendi, and V. Bulović, "Air-stable operation of transparent, colloidal quantum dot based LEDs with a unipolar device architecture," Nano Lett. **10**(1), 24–29 (2010).
25. Z. Bai, L. Hao, Z. Zhang, Z. Huang, and S. Qin, "Enhanced photoluminescence of corrugated Al2O3 film assisted by colloidal CdSe quantum dots," Nanotechnology **28**(20), 205206 (2017).
26. F. Xia, X. W. Sun, and S. Chen, "Alternating-current driven quantum-dot light-emitting diodes with high brightness," Nanoscale **11**(12), 5231–5239 (2019).
27. J. Liu, Z. Lu, X. Zhang, Y. Zhang, H. Ma, Y. Ji, X. Xu, L. Yu, J. Xu, and K. Chen, "Low power consumption red light-emitting diodes based on inorganic perovskite quantum dots under an alternating current driving mode," Nanomaterials **8**(12), 974 (2018).
28. V. Wood, M. J. Panzer, J. Chen, M. S. Bradley, J. E. Halpert, M. C. Bawendi, and V. Bulović, "Inkjet-printed quantum dot-polymer composites for full-color AC-driven displays," Adv. Mater. **21**(21), 2151–2155 (2009).

Optics EXPRESS

29. L. Wang, L. Xiao, H. Gu, and H. Sun, "Advances in Alternating Current Electroluminescent Devices," Adv. Opt. Mater. **7**(7), 1801154 (2019).
30. V. Wood, J. E. Halpert, M. J. Panzer, M. G. Bawendi, and V. Bulović, "Alternating current driven electroluminescence from ZnSe/ZnS:Mn/ZnS nanocrystals," Nano Lett. **9**(6), 2367–2371 (2009).
31. V. Wood, M. J. Panzer, D. Bozyigit, Y. Shirasaki, I. Rousseau, S. Geyer, M. G. Bawendi, and V. Bulović, "Electroluminescence from nanoscale materials via field-driven ionization," Nano Lett. **11**(7), 2927–2932 (2011).
32. S. Kobayashi, Y. Tani, and H. Kawazoe, "Quantum dot activated all-inorganic electroluminescent device fabricated using solution-synthesized CdSe/ZnS nanocrystals," Jpn. J. Appl. Phys. **46**(40), L966–L969 (2007).
33. S. S. Waje, M. W. Meshram, V. Chaudhary, R. Pandey, P. A. Mahanawar, and B. N. Thorat, "Drying and shrinkage of polymer gels," Braz. J. Chem. Eng **22**(2), 209–216 (2005).
34. A. Szanka, G. Szarka, and B. Iván, "Multi-methacrylated star-shaped, photocurable poly(methyl methacrylate) macromonomers via quasiliving ATRP with suppressed curing shrinkage," Polymer. **54**(22), 6073–6077 (2013).
35. K. Y. Kang, K. R. Hwang, J. Y. Park, J. P. Lee, J. S. Kim, and J. S. Lee, "Critical point drying: An effective drying method for direct measurement of the surface area of a pretreated cellulosic biomass," Polymers. **10**(6), 676 (2018).
36. D. H. Lee, C. T. Yuan, M. Tachiya, and J. Tang, "Influence of bin time and excitation intensity on fluorescence lifetime distribution and blinking statistics of single quantum dots," Appl. Phys. Lett. **95**(16), 163101–196 (2009).
37. L. A. Golovan, A. V. Elopov, V. B. Zaitsev, A. A. Ezhov, D. M. Zhigunov, O. N. Karpov, G. A. Shandryuk, A. S. Merekalov, and R. V. Talroze, "Photoluminescence of CdSe and CdSe/ZnS Quantum Dots in Amorphous and Liquid-Crystalline Polymer Matrices," Polym. Sci., Ser. A **62**(6), 701–713 (2020).
38. N. Reitinger, A. Hohenau, S. Köstler, J. R. Krenn, and A. Leitner, "Radiationless energy transfer in CdSe/ZnS quantum dot aggregates embedded in PMMA," Phys. Status Solidi Appl. Mater. Sci. **208**(3), 710–714 (2011).
39. E. Faulques, F. Massuyeau, Q. Wang, D. K. Seo, and S. Jobic, "Mapping emissive channels of quantum dots: Influence of size and environment on energy transfer in the time domain," Appl. Phys. Lett. **97**(15), 153111–153116 (2010).
40. H. Yu, C. Xin, Q. Zhang, M. I. B. Utama, L. Tong, and Q. H. Xiong, "II-VI compound semiconductor nanowires: Optical properties and nanophotonics," in *Semiconductor Nanowires: Materials, Synthesis, Characterization and Applications* (Elsevier Inc., 2015), pp. 29–69.
41. J.-Y. Kim, J. Yang, J. H. Yu, W. Baek, C.-H. Lee, H. J. Son, T. Hyeon, and M. J. Ko, "Highly Efficient Copper-Indium-Selenide Quantum Dot Solar Cells: Suppression of Carrier Recombination by Controlled ZnS Overlayers," ACS Nano **9**(11), 11286–11295 (2015).
42. K. Hasanirokh and A. Asgari, "Modeling and studying of white light emitting diodes based on CdS/ZnS spherical quantum dots," Opt. Mater. **81**(May), 129–133 (2018).
43. J. P. Philbin and E. Rabani, "Auger Recombination Lifetime Scaling for Type i and Quasi-Type II Core/Shell Quantum Dots," J. Phys. Chem. Lett. **11**(13), 5132–5138 (2020).